Comparative Studies on the Secondary Structure of Eukaryotic 5.8S Ribosomal RNA†

Nguyen T. Van,* Ross N. Nazar,‡ and Thomas O. Sitz§

ABSTRACT: The secondary structure of 5.8S rRNA from two widely divergent species (i.e., rat and yeast) was compared using their denaturation spectra, the derivative profiles of hypochromicity vs. temperature, and ethidium bromide probing. From denaturation spectral data, the existence of tertiary folding was observed and estimates of 70 and 60% GC in the duplex populations were obtained for Novikoff hepatoma and yeast 5.8S rRNAs, respectively. The yeast 5.8S rRNA, notwithstanding a much lower GC content, was found to possess virtually every significant structural feature observed in rat RNA. The existence of a stable stem could be demonstrated in both RNAs with derivative profiles of hyperchromicity vs. temperature, and a duplex population with a GC/AU ratio close to 1, accounting for the majority of the base pairing, was also shown to be present in both RNA species. Ethidium bromide probing data confirmed the existence of a similar degree of base pairing in rat and yeast RNAs but also showed that yeast 5.8S rRNA contains more AU pairs than the mammalian molecule. The results derived from the three techniques generally support the generalized model for mammalian 5.8S rRNA (Nazar, R. N., Sitz, T. O., and Busch, H. (1975), *J. Biol. Chem. 250,* 8591-8597) and contradict the model proposed by Rubin (Rubin, G. M. (1973), *J. Biol. Chem. 248,* 3860-3875) for yeast 5.8S rRNA in at least one important aspect, the percent of base pairing in 5.8S rRNA.

In eukaryotes the large subunit of cytoplasmic ribosomes contains a 5.8S rRNA component which is hydrogen bonded to the high-molecular-weight rRNA (Pene et al., 1968; Weinberg and Penman, 1968). The first complete nucleotide sequence of an eukaryotic 5.8S rRNA (yeast) was determined by Rubin (1973) who also proposed a model for its secondary structure (Figure 1A). More recently, the primary sequence of Novikoff hepatoma 5.8S rRNA was reported (Nazar et al., 1975) and an alternate model (Figure 1B) for eukaryotic 5.8S rRNA was suggested. The two models differ in several respects. There is 40% more base pairing (45% if only A-U and G-C base pairs are counted) in the model proposed for the Novikoff hepatoma 5.8S RNA than that proposed for yeast (Table I), although both rRNAs contain the same number of nucleotides (158 nucleotides). The base composition of the base-paired regions is also different (Table I) with the mammalian 5.8S rRNA exhibiting 73% G-C pairs vs. only 52% G-C for the yeast rRNA. This difference reflects the overall G-C contents of the two rRNA molecules (i.e., 58 and 46% for Novikoff hepatoma and yeast 5.8S RNAs, respectively).

Since 5.8S rRNA is an integral part of the eukaryotic ribosomal structure, it was reasonable to speculate that the secondary and tertiary structures of 5.8S rRNA from various species might exhibit some degree of structural similarity. Accordingly, a new estimate of the secondary structure for the yeast 5.8S rRNA sequence (Figure 1C) was proposed (Nazar et al., 1975) which was very similar to that suggested for the Novikoff hepatoma. In the new model, loop stability as dictated by the rules of Tinoco et al. (1971) was not sacrificed for the sake of maximizing similarity. In addition to the structural homologies, the new model reduced the differences in base pairing between yeast and Novikoff hepatoma 5.8S rRNAs from 36 vs. 50 base pairs (Rubin's model) to 46 vs. 50 base pairs for the generalized model (Table I). Since any estimate of the secondary structure must be substantiated by additional proofs, the present study reexamines the current models using thermal denaturation and ethidium bromide probing techniques.

Materials and Methods

Nucleic Acids and Chemicals. 5.8S ribosomal RNAs were extracted from whole cells and purified on 8% polyacrylamide gel slabs as reported earlier (Nazar et al., 1975).

Ethidium bromide was a gift from Dr. T. I. Watkins of Boots Pure Drug Co., Nottingham, England, and is of the same degree of homogeneity as the samples used by Lepecq and Paoletti (1967).

All chemicals used for buffer preparation were of reagent grade and details for preparing solutions for thermal denaturation were published earlier (Van et al., 1976).

Thermal Denaturation Technique. Details for the technique and the instrumentation required were previously reported (Van et al., 1976). Briefly, thermal denaturation of the nucleic acid solutions was performed at both 260 and 278 nm in an automated temperature-programmed, digitally recording spectrophotometer. Temperature was monitored directly by a temperature probe immersed in the sample. Data points were taken every one-third of 1° and an average experimental curve consisted of about 200 data points. Data computation and plotting were done by computer. The denaturation spectra were obtained differentially with a Cary 118 spectrophotometer as described previously (Van et al., 1975) and all data were corrected for cubic expansion of the 1 mM Tris-HCl buffer. The temperature coefficient of the molar absorbancy of the melting buffer was found to be negligible in the range 225-320 nm.

Fluorescence Measurements. Fluorescence measurements were performed in a self-constructed apparatus which included a very sensitive single photon counting system as a light de-

† From the Departments of Cell Biology and Pharmacology, Baylor College of Medicine, Houston, Texas 77030. *Received December 28, 1976.* These studies were supported by Population Center Research Grants HD 07495-04 p-8A, HD 08389, and HD 07857-06, National Institutes of Health Grant HD 08188-04, and Cancer Center Research Grant CA-10893.

‡ Present address: Division of Biological Sciences, National Research Council, Ottawa, Canada K1A OR6.

§ Present address: Department of Chemical Sciences, Old Dominion University, Norfolk, Virginia 23508.

TABLE I.

Description	Novikoff hepatoma, Generalized	Yeast	
		Rubin's model	Generalized model
Total no. of nucleotides	158	158	158
Base comp	31A, 33U, 46G, 46C, 2Ψ	41A, 43U, 37G, 36C, 1Ψ	41A, 43U, 37G, 36C, 1Ψ
AU pairs	12 (27%)[a]	15 (48.4%)[a]	20 (48.8%)[a]
GC pairs	33 (73%)[a]	16 (51.6%)[a]	21 (51.2%)[a]
Total AU, GC pairs	45 (100%)[a]	31 (100%)[a]	41 (100%)[a]
GU pairs	3	4	4
AΨ	2	1	1
Total pairs	50	36	46
% nucleotides in AU and GC pairs	57%	39%	52%
% nucleotides in all types of pairing	63%	46%	58%
% GC (overall)	58%	46%	46%
Sum of stability no.'s[b]	28[c]	16[d]	16[c]

[a] The percentage indicated in parentheses refers only to AU and GC pairs. [b] As defined by Tinoco et al. (1971). [c] Nazar et al. (1975). [d] Rubin (1973).

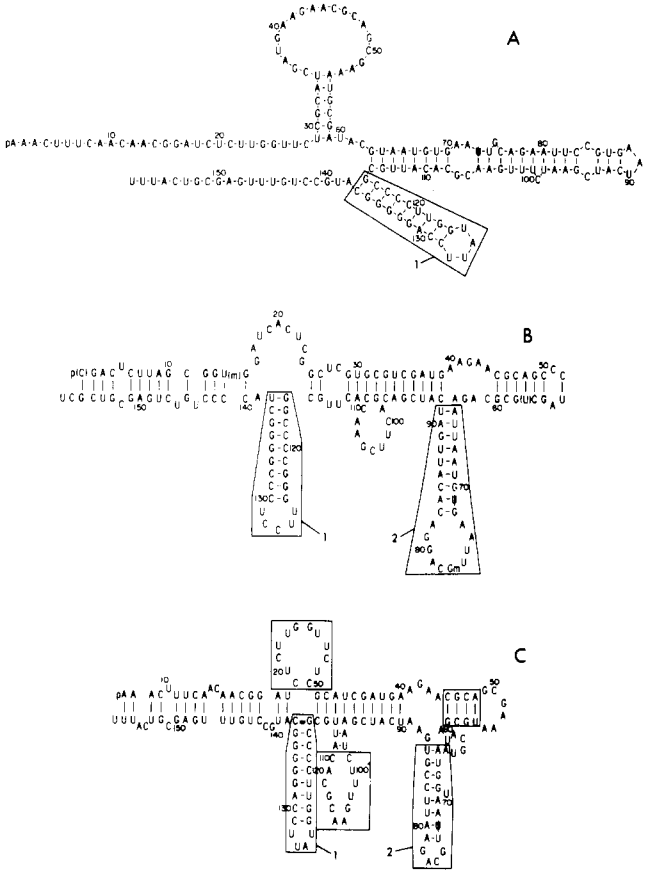

FIGURE 1: Possible secondary structures for Novikoff hepatoma and yeast 5.8S rRNAs. Boxed areas: GC-rich stems (1); AU-rich stems (2). Unnumbered boxes indicate structures in which the mammalian RNA differs the most from yeast rRNA (see text). (A) Rubin's model for yeast 5.8S rRNA; (B) Novikoff hepatoma 5.8S rRNA (model of Nazar et al.); (C) redrawn model for yeast 5.8S rRNA.

tector (Van et al., manuscript in preparation). Briefly, the nucleic acid/ethidium bromide mixtures were excited with the intense green line near 546 nm of a mercury–xenon arc lamp (1.6-nm passband). The emission monochromator was set at 590 nm (passband = 1.6 nm) and emitted photons were measured at a right angle to excitation. Samples were maintained at 25 °C to avoid a temperature effect, and readings were corrected for a blank. The latter were also normalized with respect to the nucleic acid concentration to facilitate a direct comparison. A Scatchard analysis of the data was not attempted because we were not successful in determining accurately the value of V (the fluorescence enhancement factor) for naturally occurring RNAs (Van et al., manuscript in preparation).

The fluorescence enhancement factor (V) for a nucleic acid is the ratio of the fluorescence of an ethidium bromide solution saturated with this nucleic acid to that of a solution of free ethidium bromide at identical concentration (Lepecq and Paoletti, 1967). The fluorescence enhancement capacity of a nucleic acid is the fluorescence increment produced by a given amount of this nucleic acid on a solution of ethidium bromide. The ethidium bromide concentration in this mixture is in large excess with respect to the concentration of nucleic acid. The fluorescence enhancement capacity of a nucleic acid is a function of both the concentration of strong binding sites for ethidium bromide in the latter and of the intrinsic fluorescence enhancement factor of its various binding species.

Results

(1) *Denaturation Spectra of Novikoff Hepatoma and Yeast 5.8S rRNA*

Normalized Denaturation Spectra. Fresco et al. (1963) stated that the change in molar absorbancy of a nucleic acid solution upon denaturation is linearly related to its G-C and A-U contents as follows:

$$\Delta A\lambda/c = f(\mathrm{AU}) \times \Delta A(\mathrm{AU})\lambda + f(\mathrm{GC}) \times \Delta A(\mathrm{GC})\lambda \quad (1)$$

where $\Delta A\lambda$ is the change in absorbance due to heat denaturation at wavelength λ, c is the molar concentration of the nucleic acid solution, and $f(\mathrm{AU})$ and $f(\mathrm{GC})$ are the percents of AU and GC pairs, respectively; $\Delta A(\mathrm{AU})\lambda$ and $\Delta A(\mathrm{GC})\lambda$ are the changes in molar absorbancy at wavelength λ due to the disruption of an AU or GC pair, respectively. The last two parameters are known on a molar basis (Fresco et al., 1963; Van et al., 1976; and Figure 2A) and c can be obtained from the molar absorbancy of the nucleic acid. The base composition (i.e., $f(\mathrm{AU})$ and $f(\mathrm{GC})$) of an unknown nucleic acid can therefore be determined from the knowledge of $\Delta A\lambda$ of a solution of this nucleic acid at two distinct wavelengths. Implicit in this technique is the assumption that each base pair contributes independently to the denaturation spectrum and that nearest-neighbor effects are negligible. Rewriting eq 1 for absorbance data at 260 nm:

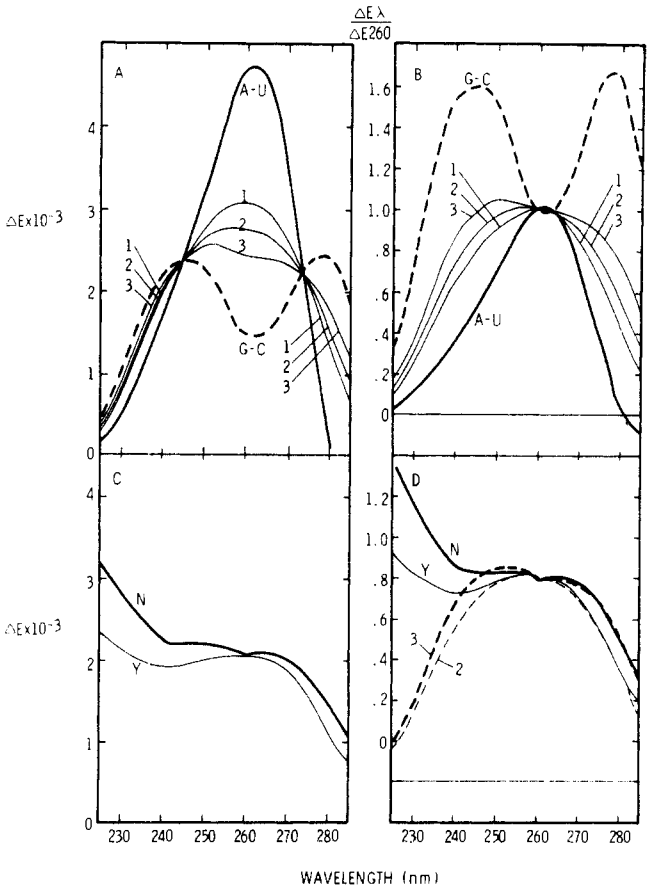

FIGURE 2: Standard and normalized denaturation spectra for AU, GC, mammalian, and yeast 5.8S rRNAs in 0.01 M KCl and 1 mM Tris buffer. (A) Standard denaturation spectra for AU and GC pairs (Van et al., 1976) and denaturation spectra computed with Fresco's eq 1 for various AU, GC pairs mixtures. Curve 1, 50% GC; curve 2, 60% GC; curve 3, 70% GC. (B) Normalized denaturation spectra for the data in Figure 2A calculated with eq 3. (C) Denaturation spectra for Novikoff hepatoma and yeast 5.8S rRNAs (unnormalized). The two areas under the denaturation spectra differ by about 6%. (D) Normalized denaturation spectra for Novikoff hepatoma and yeast 5.8S shown with the normalized denaturation spectra of AU and GC mixtures which resemble the most to the normalized denaturation spectra for the two 5.8S rRNA. N, Novikoff hepatoma 5.8S rRNA; Y, yeast 5.8S rRNA. If the integrated area under the denaturation curves in Figure 2A is plotted against GC %, the area decreases by 1.5% when the GC content increases by 10%. The denaturation spectra of the two 5.8S rRNA curve upward below 250 nm. This trend is not seen in any AU, GC mixtures shown in Figure 2A.

$$\Delta A_{260nm}/c = f(AU) \times \Delta A(AU)_{260nm} + f(GC) \times \Delta A(GC)_{260nm} \quad (2)$$

Dividing eq 2 into eq 1:

$$\Delta A\lambda/\Delta A_{260nm} = f(AU) \times (\Delta A(AU)\lambda/\sum\Delta A(AU,GC)_{260nm}) + f(GC) \times (\Delta A(GC)\lambda/\sum\Delta A(AU,GC)_{260nm}) \quad (3)$$

where $\Sigma\Delta A(AU,GC)_{260nm}$ is a shorthand for the right-hand-side expression of eq 2. This sum of products can be easily calculated for any mixture of AU and GC pairs using standard denaturation spectra for AU and GC pairs (Fresco et al., 1963; Van et al., 1976; and Figure 2A). Equation 3, therefore, simply states that the base composition (i.e., $f(AU)$ and $f(GC)$) of an unknown nucleic acid can be obtained by measuring the ratio $\Delta A\lambda/\Delta A_{260nm}$ at two distinct wavelengths of a solution of this nucleic acid. This normalized technique of presenting the hypochromicity data (hereafter referred to as normalized denaturation spectrum) has a tremendous advantage in that it permits direct comparison of denaturation spectra of naturally occurring RNA (i.e., base pairing less than 100%) to that of mixtures of AU and GC pairs (i.e., 100% paired). The wavelength 260 nm was chosen because the sensitivity of $\Delta A\lambda$ to base composition is maximized at this wavelength. A further advantage lies in the fact that it is not located on a steep slope of the absorption (or denaturation) spectra of AU, GC, or of their mixtures and therefore will minimize errors due to wavelength setting (Figure 2A). A normalized presentation of the spectra in Figure 2A is shown in Figure 2B.

Estimate of GC in the Duplexes of Mammalian and Yeast 5.8S rRNAs. The denaturation spectra and the normalized denaturation spectra of Novikoff hepatoma and yeast 5.8S rRNAs are shown in Figure 2, panels C and D, respectively. It is evident that the normalized denaturation spectra for Novikoff hepatoma and yeast 5.8S rRNAs are very similar to the normalized denaturation spectra for a mixture of 70% GC + 30% AU and 60% GC + 40% AU, respectively, but only in the wavelength range of 250-300 nm. If the estimate of the percent GC is close for the Novikoff hepatoma 5.8S rRNA (i.e., 70 vs. 73%), it is poor for the yeast 5.8S rRNA (i.e., 60 vs. 51%). A close inspection of the redrawn model for yeast 5.8S RNA indicates that 12 of the 21 AU pairs present in this model are terminal pairs (i.e., pairs that are juxtaposed to single-stranded sequences). The contribution of a terminal pair to the denaturation spectrum is likely to be less than that of an internal pair as a result of what is commonly known as terminal melting. A reverse situation exists in Novikoff hepatoma 5.8S rRNA where 14 of the 33 GC pairs are terminal pairs. This explains the lower estimate of the GC content for this RNA (i.e., 70 vs. 73%). The lower discrepancy observed with Novikoff hepatoma 5.8S rRNA is due to the fact that terminal GC pairs are also inherently more stable than terminal AU pairs.

Comparing the Extent of Base Pairing in Mammalian and Yeast 5.8S rRNAs. To estimate the percent base pairing of the two 5.8S rRNAs, we obtained the denaturation spectra for Novikoff hepatoma and yeast 5.8S rRNAs shown in Figure 2C. The area under the denaturation spectrum from 225 to 285 nm is a more accurate indicator of the amount of base pairing and base stacking in the nucleic acid than is the usual hypochromicity measured at one wavelength. Such hypochromicity is also dependent on base composition and the wavelength at which hypochromicity was observed (Van et al., 1976). It is evident that the integrated area of the denaturation spectra for Novikoff hepatoma 5.8S rRNA is only slightly larger than the corresponding area for yeast 5.8S rRNA (i.e., 6%). This result implies that the difference in the base pairing between the two 5.8S rRNAs cannot be as large as suggested by Rubin's model (i.e., 45% difference in base pairing if GU pairs are excluded). The redrawn model for the yeast 5.8S rRNA indicates the presence of 41 AU and GC pairs, and the difference in the number of base pairing in the two 5.8S rRNAs models narrows down to less then 10% (Figure 1 and Table I). Since the integrated area of the denaturation spectrum decreases by about 1.5% when the GC% of the nucleic acid increases by 10% (Figure 2A), the difference in the integrated areas of the denaturation spectra of Novikoff hepatoma and yeast 5.8S rRNAs reflects a 9% difference in base pairing. This figure is closer to the 9.7% difference in base pairing suggested by our proposed models for the two 5.8S rRNAs than to the 45% difference observed with the model proposed by Rubin. Further, the large departure between the calculated spectra and the observed spectra (Figure 2D) in the wavelength range below 250 nm must involve other forces than AU or GC base unpairing. No GC and AU combinations shown in Figure 2A

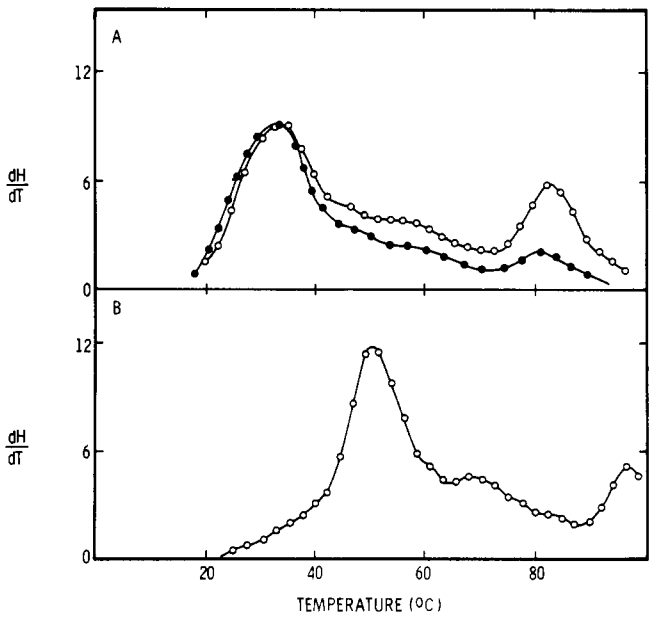

FIGURE 3: Derivative profiles of Novikoff hepatoma 5.8S rRNA at two ionic strengths. (A) dH/dT at 0.01 N KCl. T_m values of the two peaks are 34 and 82 °C, respectively. The integrated area under the 82 °C peak is 25% of the total area (278-nm profile). The integrated area under the 34 °C peak is 50% of the total area. The peak height and the area of the 82 °C peak recorded at 278 nm (open circle) are about 2.7 times the corresponding height or area of the derivative profile recorded at 260 nm (closed circle). This is an indication of the melting of very rich GC stems. (B) dH/dT at 0.1 N KCl. The T_m values of the two peaks are 51 and 96 °C, respectively. The increase in T_m with ionic concentration is about 17 and 14 °C for the low and high T_m peaks, respectively. See text for the interpretation of this data. Data are recorded at 278 nm.

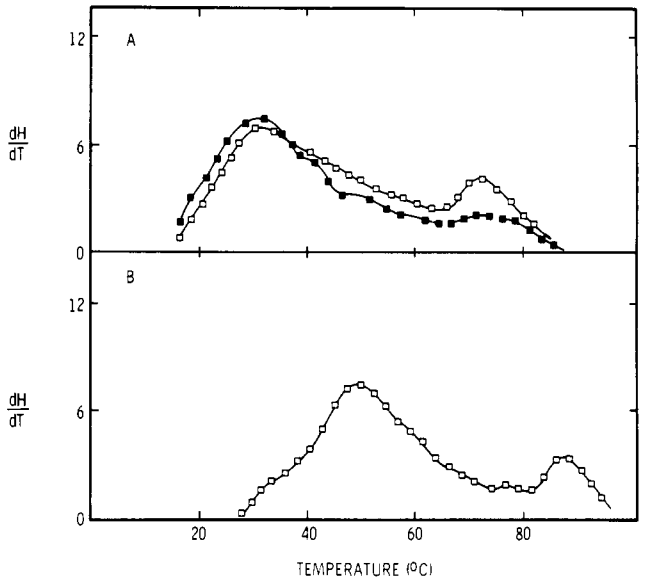

FIGURE 4: Derivative profiles of yeast 5.8S rRNA at two ionic strengths. (A) dH/dT at 0.01 N KCl. The T_m values of the two peaks are 29 and 72 °C, respectively. The integrated area under the 72 °C peak is 24% of the total area under the derivative profile at 278 nm. The peak height and the area under the 72 °C peak recorded at 278 nm (open square) are twice as high as the corresponding features recorded at 260 nm (closed square). (B) dH/dT at 0.1 N KCl. The T_m values of the two peaks are 48 and 86 °C, respectively. Data recorded at 278 nm.

can give the high $\Delta A\lambda$ observed between 220 and 240 nm with 5.8S rRNA. The unstacking of the penta-rC sequences that are present in the long GC stems of yeast and Novikoff hepatoma 5.8S rRNAs can only account for a small part of this large difference in the denaturation spectra below 250 nm. A more plausible cause for this trend in the denaturation spectra of 5.8S rRNA to curve upward below 250 nm, instead of sloping down like in Figure 2A, might be the tertiary structure. The latter is formed by additional base pairing between distant loops upon folding of the 5.8S rRNA molecule. This phenomenon, which has been observed in tRNA (Cramer and Gauss, 1972), also exhibits a large hypochromic effect that can not be accounted for by the relatively few number of base pairs contained in the generally accepted "clover-leaf" model. Therefore, the denaturation spectra for small, naturally occurring RNA, such as tRNA and 5.8S rRNA, exhibit the effect of tertiary structure in addition to the effect of base pairing. If one accepts that similar tertiary structure would have approximately the same effect on the denaturation spectra, the difference in the integrated area of the denaturation spectra of RNA of the same type (i.e., 5.8S rRNA or tRNA) reflects mainly the difference in base pairing.

(2) *Derivative Profiles of the Thermal Denaturation Transitions for Novikoff Hepatoma and Yeast 5.8S rRNAs*

The denaturation spectra shown earlier (Figure 2C,D) left unanswered the question of how G-C and A-U pairs are distributed in different duplex populations which constitute the secondary structure of the two 5.8S rRNAs. However, thermal denaturation profiles, especially when presented as the derivative of H, the hypochromicity vs. temperature, can demonstrate the presence of various duplex populations of different base composition or length, since these duplex populations differ by their thermal stability.

Derivative Profiles for Novikoff Hepatoma 5.8S rRNA. The thermal denaturation curves and the resulting derivative profiles of Novikoff hepatoma 5.8S recorded at 260 and 278 nm are shown in Figure 3. Corresponding data for yeast 5.8S rRNA are shown in Figure 4. At low ionic strength, the derivative profile at 278 nm for Novikoff hepatoma 5.8S rRNA shows two distinct peaks with T_m at 34 and 82 °C, respectively. The portion of the derivative profile between the two peaks consists of overlapping peaks which can be resolved into at least three more gaussian peaks. When the derivative profile at 278 nm is compared to the derivative profile at 260 nm (which maximizes the contribution from AU pairs), the height and the shape of the low T_m peaks (34 °C) are about the same.

Identification of Features in the Derivative Profiles with Secondary Structure. The ratio of $(dH/dT)_{278nm}/(dH/dT)_{260nm}$ increases gradually from 1.1 to 2.7 when the temperature varies from 40 to 82 °C. A higher than unity peak-height ratio has been identified with a G-C rich composition of the duplex population (Van et al., 1976). The almost three times larger 82 °C peak observed when the derivative profile recorded at 278 nm was compared to the corresponding peak at 260 nm suggests that the peak at 82 °C corresponds to the melting of very rich GC stems. An inspection of our proposed model for Novikoff hepatoma 5.8S rRNA indicates that this 82 °C peak might correspond to the melting of the GC-rich stem which is formed by a hairpin loop involving residues 116 to 138. This stem contains eight uninterrupted G-C pairs, one G-U pair, and one 5-nucleotide loop. The GC percent of the paired components of this stem is close to 90%, thus making it a very likely candidate for the high temperature peak at 82 °C. At 0.1 N KCl, the T_m of the GC-rich stem is 96 °C (Figure 3B). The Novikoff hepatoma 5.8S rRNA is thus not completely denatured at 100 °C when the ionic strength exceeds 0.1 N KCl. When the ionic strength changes by 1 decade of concentration (i.e., from 0.01 to 0.1 N KCl), the T_m of the

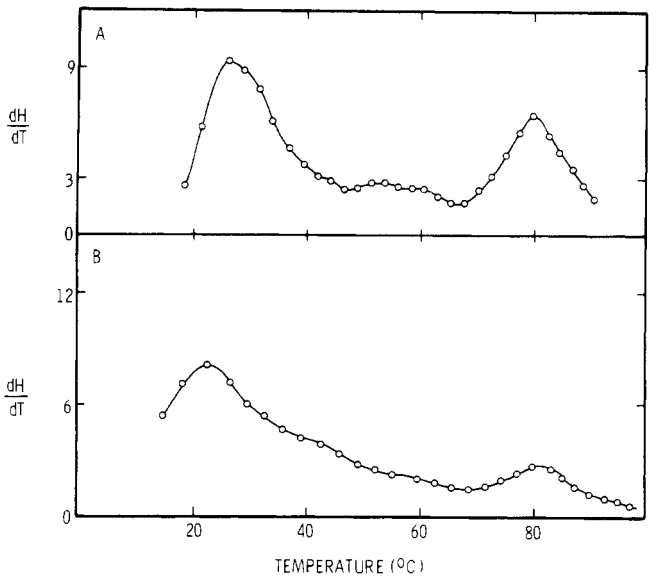

FIGURE 5: Derivative profiles of Novikoff hepatoma 5.8S rRNA in 50% formamide and 30% glycerol at 278 nm. (A) 50% formamide, 0.02 N KCl; (B) 30% glycerol, 0.02 N KCl.

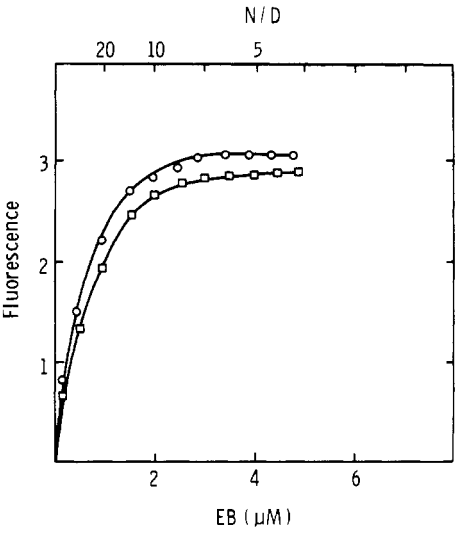

FIGURE 6: Ethidium bromide titration curves for Novikoff hepatoma and yeast 5.8S rRNAs. RNA concentration = 15 μM; buffer = 0.1 N KCl; Novikoff hepatoma = open circle; yeast = open square; abscissa axis = top = ratio of ethidium bromide molar concentration to RNA concentration (as phosphate); bottom = ethidium bromide concentration; fluorescence units: photons $\times 10^{-4}$/s.

thermolabile peak increases by 17 °C, whereas the T_m of the GC-rich peak increases only by 14 °C. This thermolabile peak does not correspond to the melting of any single stem of our proposed model, since its integrated area accounts for 50% of the total area. It is likely that it corresponds to the simultaneous melting of the AU-rich stem (residues 64 to 91) and several shorter stems containing both AU and GC pairs. The melting of the intermediate portion between 34 and 82 °C might correspond to the denaturation of residues 45–60 which contain five GC pairs and probably from part of a stem formed by the pairing of residues 12 to 15 and residues 140 to 143. This stem contains an additional three GC pairs.

Similarity in the Thermal Data of Mammalian and Yeast 5.8S rRNAs. The derivative profiles of yeast 5.8S rRNA indicate a large similarity with the corresponding profile for Novikoff hepatoma 5.8S rRNA (Figure 4). This similarity is the more remarkable if one takes into account the large difference in GC content of the two 5.8S rRNAs. We note particularly the presence of both the low T_m peak (29 °C) and the thermostable peak (T_m = 72 °C). The T_m values of these two peaks increase to 48 and 86 °C, respectively, when the ionic strength increases to 0.1 M KCl. The high GC peak is less thermostable than the GC peak in Novikoff hepatoma. This was due to the presence of destabilizing base pairs AU and GU in the long stretch of GC pairs in yeast 5.8S rRNA.

Influence of Tertiary Folding on Thermal Denaturation Data. Since the hypochromicity (as measured by the integrated area under the denaturation spectrum) of Novikoff hepatoma and yeast 5.8S rRNAs is much larger than that expected for an RNA with 52–57% base pairing, we have suggested (section 1) that this discrepancy might be due to tertiary folding. The contribution of tertiary folding on thermal denaturation data is difficult to quantitate. We have attempted to get an indirect answer to this problem by denaturing Novikoff hepatoma 5.8S rRNA in the presence of agents, such as glycerol, urea, and formamide, which are known to disturb tertiary structure. The derivative profiles of such experiments are shown in Figure 5. It is evident that all the structural features already observed with the conventional aqueous melting buffer are still present when the melting buffer also contains 50% formamide or 30% glycerol. The only difference is the expected lower T_m noted for various peaks. This result is interpreted to mean that the thermal denaturation data above 250 nm are not influenced by tertiary folding, at least not significantly.

Fluorescence Probing of Novikoff Hepatoma and Yeast 5.8S RNAs. Lepecq and Paoletti (1967) have shown that the trypanocidal drug ethidium bromide might be used as a molecular probe to estimate base pairing in naturally occurring RNA. The basis of this technique is the fluorescence enhancement of ethidium bromide caused by binding to the duplex regions of nucleic acids. Accordingly, we obtained the complete ethidium bromide binding curves for Novikoff hepatoma and yeast 5.8S rRNAs (Figure 6). It is interesting to note that the fluorescence enhancement of ethidium bromide is larger for the yeast rRNA than for the mammalian 5.8S rRNA in both respects: initial slope of fluorescence increment vs. amount of ethidium bromide added and magnitude of the fluorescence enhancement at saturation of the RNA by the drug. This result is puzzling, since if the classical interpretation of ethidium bromide binding is correct then yeast 5.8S rRNA should contain more "strong" binding sites (i.e., sites that can intercalate between base pair planes, in other words, more base pairing) endowed with large fluorescence enhancement capacity than Novikoff hepatoma 5.8S rRNA (Lepecq and Paoletti, 1967). In this case, the ethidium bromide binding data is in contradiction with not only our proposed secondary structure models for 5.8S rRNA but also with the thermal denaturation data. However, we have found that the fluorescence enhancement factor V of A-U pairs was more than twice that of G-C pairs (Van et al., manuscript in preparation). It appears that the higher fluorescence enhancement level achieved with yeast rRNA (Figure 6) compared to that of mammalian rRNA was due to a higher concentration of (A-U) pairs present in the former than in the latter (Table I). It should be noted that in the presence of an excess of ethidium bromide, the normally unstable "terminal" AU pairs are stabilized (as evidenced by a 12 °C increase in T_m of the thermolabile peak in Figure 3A when the melting buffer contains 3 μM ethidium bromide in addition to 0.01 M KCl (data not shown)).

Discussion

Current models for the secondary structure of eukaryotic 5.8S rRNA (Figure 1) have been evaluated using thermal

denaturation and ethidium bromide probing techniques. The results generally support the model proposed for mammalian 5.8S rRNA (Nazar et al., 1975) and contradict the estimate proposed for yeast 5.8S rRNA (Rubin 1973) in at least one important aspect, the percent of base pairing.

The physical measurements, however, were not completely consistent with any of the present models. Several points, such as the upward turn of the denaturation spectra below 250 nm and the larger than predicted hypochromicity of the two 5.8S rRNAs, might be due to the tertiary folding of the RNA molecules. Unfortunately, if this is the explanation, we still cannot quantitatively determine the relative contributions of tertiary and secondary structure to these physical parameters. Nevertheless, the thermal denaturation of the RNAs in buffers containing agents that are known to disturb at least tertiary structure is also in full agreement with the melting data obtained using the conventional buffer. The estimate of 70% GC in the duplex populations of Novikoff hepatoma 5.8S rRNA is valid, since the agreement between the denaturation spectrum of this RNA and the calculated spectrum for the 70% GC + 30% AU mixture above 250 nm is almost perfect. However, when the same technique was applied to yeast 5.8S rRNA, it yielded poor results. The fact that more than half of the AU pairs in yeast 5.8S rRNA are "terminal" pairs might account for this discrepancy.

The existence of a GC-rich stem in both 5.8S rRNAs is convincingly established in all buffer systems. The broad thermolabile peaks resulted from the melting of a duplex population richer in AU (this fact is attested to not only by the low T_m of these peaks but also by the larger change in the T_m with ionic strength (Van et al., 1976)). The simultaneous melting of the mixture of the AU-rich stem and various short AU and GC stems can account for the low T_m peak in both Novikoff hepatoma and yeast 5.8S rRNA. The fact that the total GC base pairs contribution to this mixture must be close to 50–54% is attested to by the similarity of the derivative profile at 260 and 278 nm in the relevant temperature range (Van et al., 1976). The inspection of the two models suggests that such a mixture with GC pair % close to 50–54% is present in both models and can quantitatively account for the integrated area under the low T_m peak of the derivative profiles. The ethidium bromide study also provides the picture that both 5.8S rRNAs are substantially and equally base paired but there are about twice as many AU pairs in the yeast 5.8S rRNA than in the mammalian rRNA.

As has been argued for the secondary structure, a common role for 5.8S rRNA in ribosome structure or function would predict some conservation of tertiary structure during evolution giving rise to common binding sites for RNA or protein on the surface of the folded molecule. All known tRNA sequences can be arranged into a "clover-leaf" model and these can assume well-defined three-dimensional configurations (Crammer and Gauss, 1972). By analogy, the generalized model for 5.8S rRNA (Nazar et al., 1975) appears to provide a homologous secondary structure, which the denaturation spectra, particularly below 250 nm, and the large hypochromicity suggest may further assume a similar three-dimensional configuration. Further studies utilizing x-ray diffraction or nuclear magnetic resonance will be required to establish a conserved tertiary structure. Additional information concerning nucleotide sequences for other eukaryotes will also be required to verify such a generalized model.

Finally, it is interesting to note that greater stability appears to be sought in the course of evolution. Not only does the overall GC percent increase from 46% for the yeast rRNA to 58% for Novikoff hepatoma 5.8S rRNA, but the replacement of destabilizing pairs (AU and GU) by GC pairs in the long GC stems (residues 116–137, stem; and residues 45–59, hairpin in the yeast 5.8S rRNA model) further stabilizes significant structural features of 5.8S rRNA. Therefore, the T_m of the high GC arm of the mammalian RNA is increased by about 10 °C with respect to the corresponding peak of the yeast 5.8S RNA. The sizes of two single-stranded loops (residues 19–30 and 98–110 in the model of Nazar et al. for yeast 5.8S rRNA) are also reduced by about 30% in the mammalian RNA. Since a long single-stranded loop is synonymous with wandering and less rigid conformation (the open loop can possess accurate "secondary" structure due to base stacking (Dube et al., 1969)), a reduction in the number of nucleotides noted in the open loops of Novikoff hepatoma 5.8S rRNA is also in line with the evolutionary concept after which a functional macromolecule in a higher organism is like a precision part in a complicated machinery which does not tolerate loose fit. This reduction in the size of the single-stranded loops cannot proceed ad infinitum. We believe that loop size will remain stable when the number of nucleotides in the loop reaches an optimum value, probably between 4 and 6. Another significant feature is the similar emplacement of the AΨ pair in the AU-rich hairpin of both 5.8S rRNAs. It might be eventually proven that this AΨ-pair emplacement is significant, such as been observed with tRNA (Zachau, 1972).

Acknowledgment

The authors thank Drs. B. W. O'Malley and H. Busch for helpful discussions and support, R. K. Busch for supplying the Novikoff hepatoma bearing rats, J. M. Delaney for proofing the manuscript, and Tim Yu for excellent technical assistance.

References

Cramer, F., and Gauss, D. H. (1972), *Front. Biol. 27*, 173–217.

Dube, S. K., Rudland, P. S., Clark, B. F. C., and Marker, K. A. (1969), *Cold Spring Harbor Symp. Quant. Biol. 34*, 161–166.

Fresco, J. R., Klotz, L. C., and Richards, E. G. (1963), *Cold Spring Harbor Symp. Quant. Biol. 28*, 83–90.

Le Pecq, J. B., and Paoletti, C. (1967), *J. Mol. Biol. 27*, 87–106.

Nazar, R. N., Sitz, T. O., and Busch, H. (1975), *J. Biol. Chem. 250*, 8591–8597.

Pene, J. J., Knight, E., Jr., and Darnell, J. E., Jr. (1968), *J. Mol. Biol. 33*, 609–623.

Rubin, G. M. (1973), *J. Biol. Chem. 248*, 3860–3875.

Tinoco, I., Jr., Uhlenbeck, O. C., and Levine, M. D. (1971), *Nature (London) 230*, 362–367.

Van, N. T., Holder, J. W., Woo, S. L. C., Means, A. R., and O'Malley, B. W. (1976), *Biochemistry 15*, 2054–2062.

Weinberg, R. A., and Penman, S. (1968), *J. Mol. Biol. 38*, 289–304.

Zachau, H. G. (1972), *Front. Biol. 27*, 173–217.